Control of liquefaction induced settlement of buildings using basement structures

F. Hughes & S. P. G. Madabhushi
Department of Engineering - University of Cambridge, Cambridge, United Kingdom

ABSTRACT
It is important for geotechnical engineers to design to control settlements of structures. This point has become more significant with the rapid increase in performance based design in geotechnical engineering. Presented here are the initial findings of an investigation looking at controlling the liquefaction induced settlement of buildings using basement structures. Liquefaction induced uplift of buried structures has been observed in previous earthquakes, including the uplift of shrimp farm tanks in Pedernales, Ecuador, after the April 2016 Muisne earthquake. This observation can be used to reduce settlement of structures with shallow foundations. The basic premise for this research is that it may be cost effective to include basements for structures, especially in densely populated cities, to mitigate liquefaction induced settlements. The inclusion of basements can provide uplift forces during the liquefied period thereby reducing settlement of the structures.

A series of dynamic geotechnical centrifuge tests are currently being conducted at the University of Cambridge to investigate the effect of the presence of a basement structure on a building sited on liquefiable soil. The starting point for these tests was to investigate the behavior of a structure with a total weight equal to the uplift provided by its basement when the surrounding soil liquefies. By vertical force equilibrium, this structure should neither settle nor float. A single degree of freedom sway frame rigidly connected to a stiff basement structure was used. The dynamic response of the structure and the surrounding soil were monitored in the pre, during, and post liquefaction periods. Data from the first of these test is presented in this paper.

1 INTRODUCTION

Liquefaction is continuing to be a cause of major damage in earthquakes in locations across the world, including, for example, the 2016 Muisne, Ecuador earthquake. This highlights the imperative need for further research into earthquake induced liquefaction and associated damage, particularly regarding effective and affordable mitigation methods.

Liquefaction induced settlement and rotation of structures on flat ground results from the combined effect of volumetric and deviatoric induced deformations which occur during both the co- and post- seismic periods (Dashti et al. 2010). The mechanisms of displacement are sensitive to an extensive number of parameters, most notably seismic demand, structure bearing pressure, sand relative density and liquefiable layer thickness. Damage to structures and the associated losses are greatest when differential displacement occurs across the structure and between the structure and adjoining infrastructure.

Liquefaction has also been observed to cause damage to underground structures in flat ground such as pipelines and storage tanks, whereby the structures float due to having a lower unit weight than the liquefied soil surrounding them (Koseki et al. 1997; Chian & Madabhushi 2012). Differential settlement of pipelines due to liquefaction can cause damage to vital distribution networks (O'Rourke et al. 2014).

A number of methods are currently used to reduce or remove the risk of earthquake induced liquefaction and the associated damage to surface and underground structures. For example, structural settlement can be reduced through soil improvement (Mitrani & Madabhushi 2010) or reducing the degree of saturation in the soil (Zeybek & Madabhushi 2016). However, these methods have the effect of amplifying the accelerations transmitted to the structure.

Intuitively, problems experienced by surface structures settling and subsurface structures floating due to earthquake induced liquefaction can counterbalance each other and be combined to reduce the displacement of structures. Presented here are the design and findings of the first set of a series of dynamic centrifuge tests which have been conducted to investigate whether the buoyancy provided by basement structures when the surrounding soil liquefies can be used to reduce the settlement of structures.

2 FIELD OBSERVATIONS

The first author was part of a seven person reconnaissance mission deployed in Ecuador by the Earthquake Engineering Field Investigation Team (EEFIT) following the April 16th 2016 M_w = 7.8 earthquake (Franco et al. 2017).

The damage to a shrimp farm on the sea front in Pedernales (Figure 1), 36 km south-south-west of the epicenter, is believed to have been caused by earthquake induced liquefaction. A structure with underground storage tanks which were empty at the time of the earthquake experienced relative uplift compared to the structures adjacent to it, which did not have underground storage tanks. Relative uplifts of 210 mm and 120 mm were measured relative to the adjacent structures (Figure 2) however, absolute settlements are not known due to the surrounding ground having settled. The structure with subsurface storage tanks can be likened to a one storey

structure with a basement. This implies that it is possible to reduce liquefaction induced structural settlement using basement storeys. Whilst it is not possible to infer the effects of a basement on taller or heavier structures, the behaviour of this shrimp farm suggests that it is an avenue which is worthwhile investigating.

Figure 1: Drone image of position of shrimp farm on the sea front in Pedernales, with the red rectangle identifying the structure with underground storage tanks.

Figure 2: Relative uplift of structure with underground storage tanks at Pedernales shrimp farm.

3 EXPERIMENTAL METHODOLOGY

Dynamic centrifuge experiments were performed on the Turner Beam Centrifuge at the Schofield Centre of the University of Cambridge (Schofield 1980). The tests were conducted in a laminar box (Brennan et al. 2006). A liquefiable layer of loose sand, with a relative density of 43%, was prepared by air pluviation of Hostun sand using an automatic sand pourer (Madabhushi et al. 2006). Properties of Hostun sand are given in Table 1. The tests were conducted at 60 g. A high viscosity aqueous solution of hydroxypropyl methycellulose with a viscosity of 60 cSt was used as the pore fluid to address the inconsistency between the scaling laws of dynamic and seepage time in centrifuge modeling (Schofield 1981). Piezoelectric accelerometers, micro electro-mechanical system accelerometers (MEMS), pore pressure transducers (PPTs), and linear variable displacement transducers (LVDTs) were used. Their locations are shown in Figure 3. A stored-angular momentum (SAM) actuator was used to generate sinusoidal input motions (Madabhushi et al. 1998). The characteristics of the fired earthquakes discussed in this paper are given in Table 2.

Table 1. Properties of Hostun sand (Mitrani & Madabhushi 2010)

Property	Value
e_{max}	1.01
e_{min}	0.555
G_s	2.65

Table 2. Characteristics of input motion (prototype scale)

Earthquake	PGA (g)	D_{5-95} (s)	Freq (Hz)
A	0.09	11.6	1
B	0.37	20.2	1

Table 3. Structural properties (prototype scale)

Property	Value
Bearing pressure (static) (kPa)	33.4
Superstructure height (m)	6.7
Basement depth (m)	3.9
Basement width (m)	4.5
Fixed base natural frequency (Hz)	1

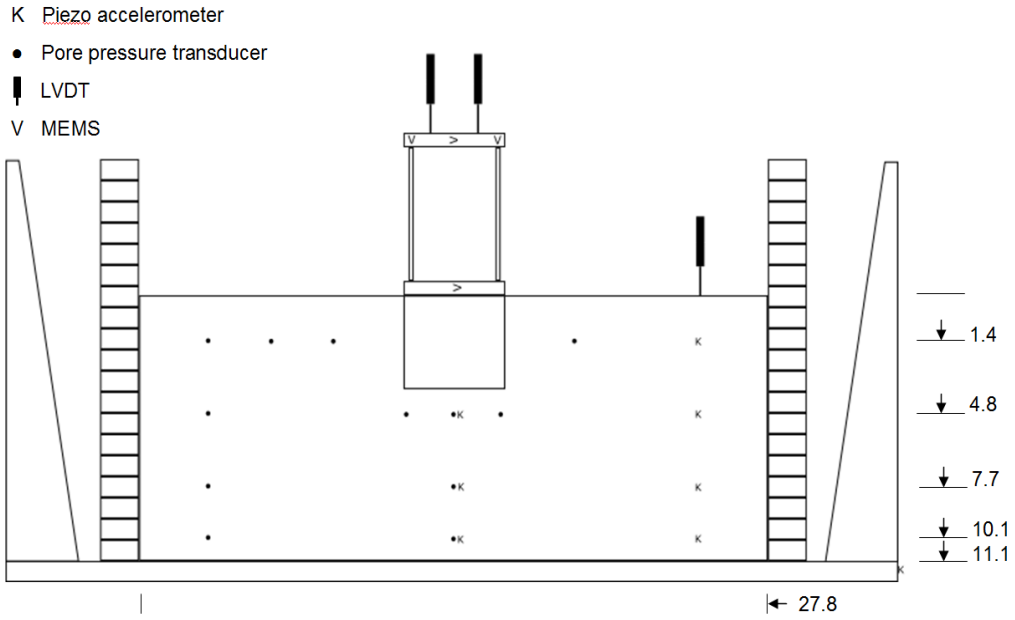

Figure 3: Cross section of centrifuge model layout showing locations of instrumentation (dimensions in m at prototype scale).

The structure consisted of a single degree of freedom (SDOF) sway frame rigidly connected to a rigid basement structure which was constructed out of sheet aluminum surrounding closed-cell foam. Structural properties are given in Table 3.

4 BASEMENT DESIGN

The basement of the structure was designed to provide an uplift force equal to the weight of the structure when the surrounding soil liquefies, resulting in neutral buoyancy in the event of soil liquefaction. This design philosophy is similar to that of "floating" or "compensated" foundations used to reduce structural settlement in locations with soft soil conditions (Tomlinson 2001), and can also be likened to the design of boats.

Vertical forces acting on the structure in static and dynamic conditions are shown in Figure 4. In static conditions, the uplift force due to buoyancy ($F_{U,H}$) is resisted by the weight of the superstructure and basement (F_S and F_B respectively) and the shear resistance along the soil-structure interface (F_F). In the event of soil liquefaction, the shear resistance of the soil reduces significantly so the shear resistance along the soil-structure interface is assumed to be negligible (Koseki et al. 1997). In addition, the uplift force acting on the structure ($F_{U,L}$) increases to greater than the hydrostatic value ($F_{U,H}$). This can be considered in two ways. Firstly, excess pore pressures are generated and act on the bottom of the basement in addition to the hydrostatic pressure present in the static analysis. Alternatively, the total uplift force can be calculated using Archimedes' principle, assuming the soil behaves as a viscous fluid when liquefied. These methods are equivalent when liquefaction occurs and the excess pore pressure generated is equal in magnitude to the initial vertical effective stress in the soil.

For neutral buoyancy in the event of soil liquefaction,

$$F_{U,L} = F_S + F_B \quad [1]$$

Where $F_{U,L}$ is the uplift force when soil liquefaction occurs, and F_S and F_B are the weights of the superstructure and basement respectively.

Archimedes' principle states that any body completely or partially submerged in a fluid at rest is acted upon by an upward, buoyant force, the magnitude of which is equal to the weight of the fluid displaced by the body. Assuming that the liquefied soil acts as a viscous fluid, Archimedes' principle can be used to calculate the uplift provided by the basement.

$$F_{U,L} = \gamma_{sat} \times V_{basement} \quad [2]$$

Where γ_{sat} is the saturated unit weight of the soil and $V_{basement}$ is the volume of the basement below the ground surface, which is equal to the depth of the basement (d) multiplied by the cross sectional area (A).

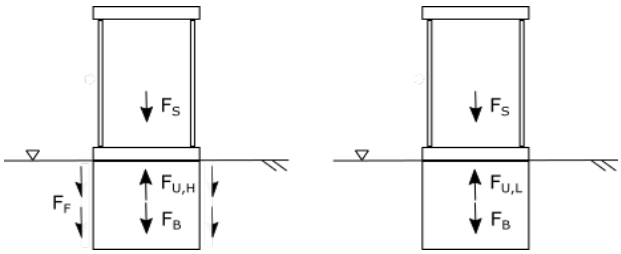

(a) (b)

Figure 4. Vertical forces acting on structure with a basement (a) static conditions, (b) in the event of complete soil liquefaction.

The depth of basement required for neutral buoyancy, $d_{neutral}$ can therefore be calculated.

$$d_{neutral} = \frac{F_{U,L}}{\gamma_{sat} \times A_{basement}} \quad [3]$$

In static conditions, the bearing pressure under the structure,

$$q_{static} = \frac{F_S + F_B - F_{U,H}}{A_{basement}} \quad [4]$$

At an equal depth below the ground surface in the far-field, the vertical effective stress

$$\sigma'_v = (\gamma_{sat} - \gamma_w) \times d_{neutral} \quad [5]$$

Therefore, when the basement is designed to achieve neutral buoyancy,

$$q_{static} = \frac{F_S + F_B - F_{U,H}}{A_{basement}} = \frac{F_{U,L} - F_{U,H}}{A_{basement}} = \sigma'_V \quad [6]$$

Consequently, the bearing pressure under the structure is equal to the effective stress in the far-field at the same depth below the ground surface.

In the event of soil liquefaction

$$q_{liquefaction} = \frac{F_S + F_B - F_{U,L}}{A_{basement}} \quad [7]$$

When the basement of the structure is designed to achieve neutral buoyancy (Equation 1 is fulfilled) and soil liquefaction occurs, the bearing pressure below a structure with neutral buoyancy will become nearly zero.

5 RESULTS AND DISCUSSION

All numerical quantities stated correspond to prototype scale, unless otherwise stated.

5.1 Structural and far-field displacement

Structural and far-field displacements were monitored during the earthquakes, and are shown in Table 4 and Figure 5. A negative displacement corresponds to settlement and a positive displacement corresponds to floatation. The rate of displacement was greatest in the co-seismic period, which is consistent with previously published centrifuge model test data for both surface and subsurface structures (Dashti et al. 2010; Madabhushi & Haigh 2012). In both earthquakes, the far-field surface settled; 53.1 mm and 171.9 mm in earthquakes A and B respectively. In comparison, movement of the structure was minimal in earthquake A, and the structure floated in earthquake B (119.6mm peak, 79.5 mm residual). In earthquake B the structure continued to float in the post-seismic period, followed by settlement when excess pore pressures began to dissipate adjacent to the basement. At this time the uplift force acting on the structure is decreasing and the frictional resistance opposing uplift increases (Figure 4).

Structures on shallow foundations sited on liquefiable soil have been observed to experience greater settlement than the far-field soil, both in the field and in centrifuge model tests (Bertalot et al. 2013). In the tests presented in the current paper, the presence of a basement prevents the structure settling more than the far-field. However, the structure uplifted, which is also undesirable. The optimum case would be such that the structure settles the same amount as the surrounding ground, so that relative displacements are negligible.

Table 4. Structural and far-field displacements.

Displacement (mm)	Earthquake A		Earthquake B	
	Structure	Far-field	Structure	Far-field
Seismic	6.3 ↑	36.0 ↓	29.7 ↑	102.9 ↓
Post-seismic	8.9 ↓	17.1 ↓	49.8 ↑	69.0 ↓
Overall accumulated	2.6 ↓	53.1 ↓	79.5 ↑	171.9 ↓

N.B. Arrows indicate direction of displacement.

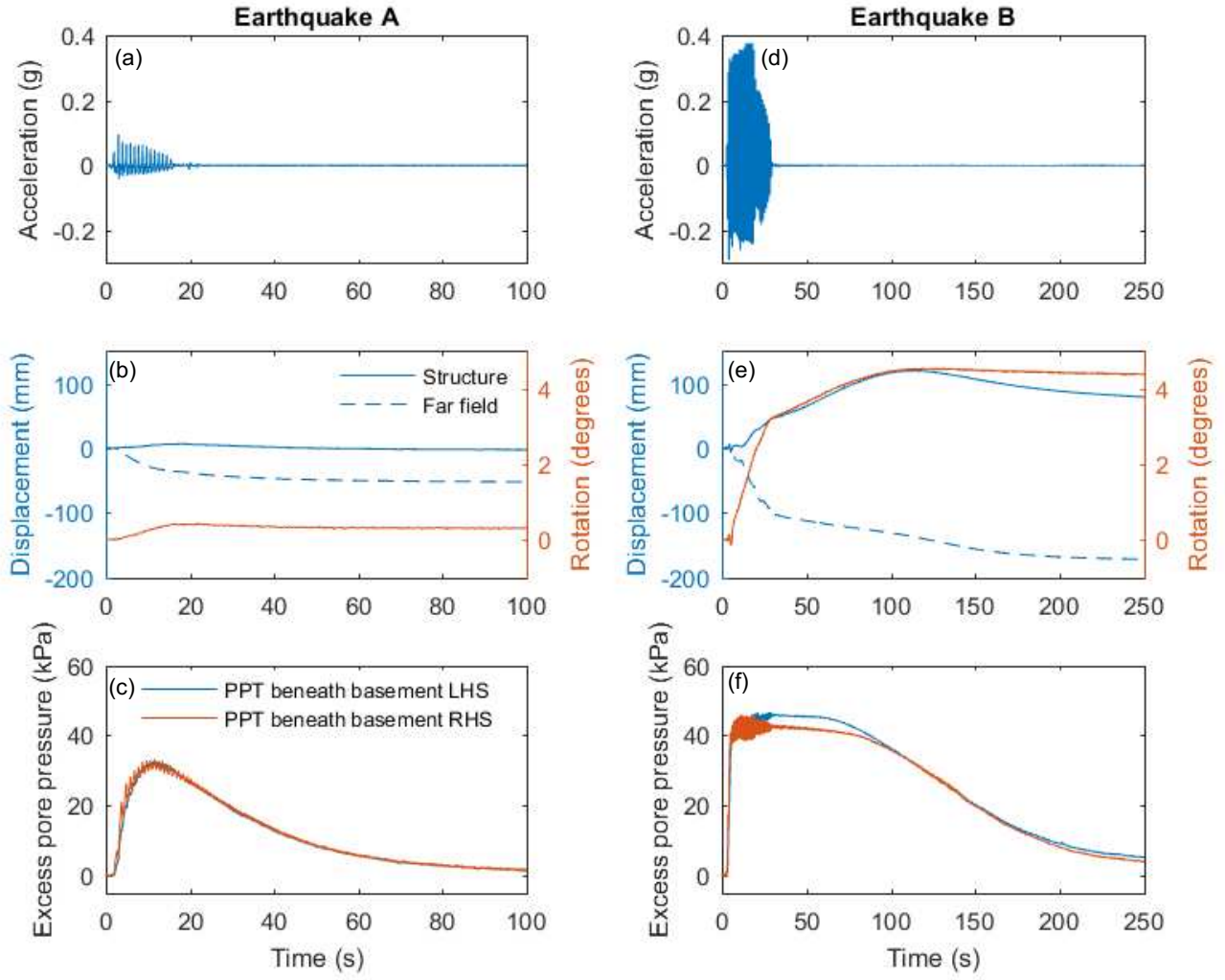

Figure 5. Comparison of structural behaviour in earthquakes A and B. Negative displacement corresponds to settlement and positive displacement corresponds to uplift. Positive rotation is anticlockwise. (a) Earthquake A input motion, (b) Displacement and rotation during earthquake A, (c) Excess pore pressure underneath the left and right hand edges of the basement during earthquake A, (d) Earthquake B input motion, (e) Displacement and rotation during earthquake B, (f) Excess pore pressure underneath the left and right hand edges of the basement during earthquake B.

During earthquake B, the excess pore pressure measured underneath the right hand edge of the structure reduces as the structure uplifts and rotates due to the formation of extensile stress. In contrast, the excess pore pressure increases under the left hand side of the structure. It is anticipated that a "no-breakaway" condition occurs underneath the basement, which is expected to occur in less permeable soil and when the loading rate is high (Allmond & Kutter 2014). Instead of a gap being formed below the basement when the structure uplifts, the drop in excess pore pressure causes the liquefied soil to move with the uplifting structure. Sand accumulates below the basement, resulting in permanent uplift and rotation of the structure (Figure 5). If a gap were to be formed underneath the structure the post-seismic settlement of the structure would be expected to be greater than that in the far-field, with the structure moving back into the void it formed. Figure 5 and Table 4 show that the structure continues to uplift when the shaking stops, before settling at a similar rate as the far-field when excess pore pressures dissipate.

5.2 Soil stress - strain behavior

The cyclic shear stress and shear strain at the mid point between accelerometer pairs aligned in vertical columns were calculated (Brennan et al. 2005). Acceleration data obtained during the centrifuge test was band pass filtered

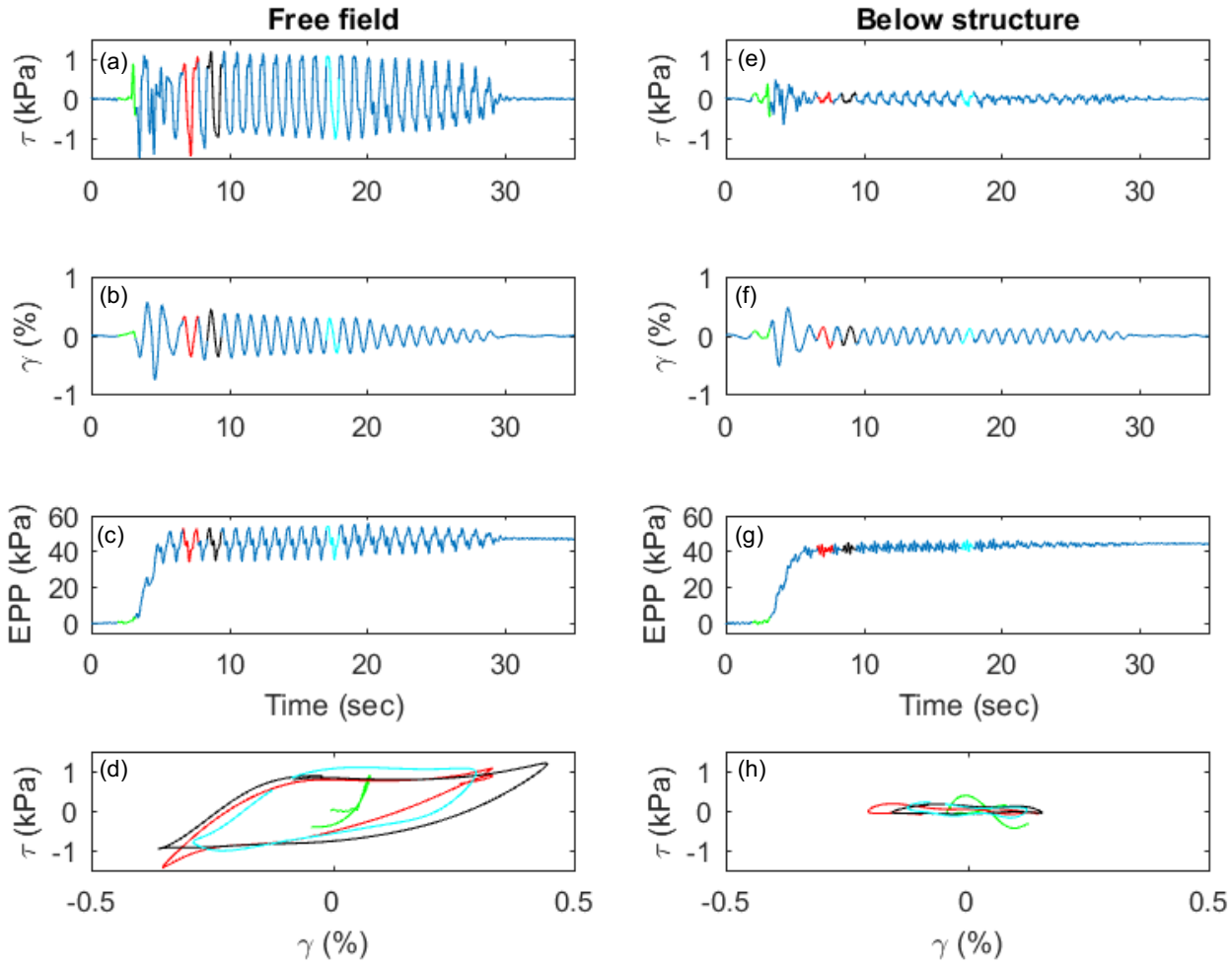

Figure 6. Comparison of soil behaviour during earthquake B, at a depth of 6.25 m both below the ground surface in the far-field and below the structure. Green, red, black and cyan colour is used to identify individual cycles during the shaking. (a) Shear stress time history in the far-field, (b) Shear strain time history in the far-field, (c) Excess pore pressure time history in the far-field, (d) Stress-strain loops for selected cycles in the far-field, where the colours identify which period the cycles correspond to, (e) Shear stress time history underneath the structure, (f) Shear strain time history underneath the structure, (g) Excess pore pressure time history underneath the structure, (h) Stress-strain loops for selected cycles underneath the structure, where the colours identify which period the cycles correspond to.

prior to integration to obtain velocity and then again prior to integration to obtain displacements. It is possible that accelerometers moved vertically during the test, sinking in the liquefied soil. It was not possible to monitor the vertical movement of the accelerometers during each earthquake therefore, they are assumed to remain in their initial position throughout the test. Figure 6 shows the soil behavior during earthquake B at a depth of 6.25 m below the ground surface, both in the far-field and underneath the structure.

When earthquake shaking begins, excess pore pressures are generated as the tendency of the loose soil skeleton to contract is prevented by the pore fluid (Figure 6 c and g). The moving average excess pore pressures generated in the far-field and under the structure are the same. This is due to the same initial effective stress at both locations. In both locations liquefaction occurred.

The initial, pre liquefaction cycle of shear strain in the far-field and underneath the structure are of comparable amplitude (Figure 6 b and f). However, the amplitude of subsequent cycles is significantly greater in the far-field than underneath the structure. This results in the soil skeleton having a greater tendency to dilate in the far-field than underneath the structure, shown by the greater peak to peak range of excess pore pressure in the co-seismic period. This can lead to a temporary increase in shear strength of the soil. This is consistent with Figures 6 d and h showing the shear stress – shear strain behavior of the

soil. The shear modulus, which can be evaluated as the ratio of the difference in maximum and minimum stress during a cycle to the difference in the maximum and minimum strain developed in that cycle, is greater in the far-field where the cyclic shear strain has a greater amplitude. Underneath the structure, the cyclic shear stress-strain loops are almost horizontal, indicating a near zero shear modulus.

6 CONCLUSION

The relative uplift of a shrimp farm with underground storage tanks compared to adjacent structures after the M_w = 7.8 Muisne earthquake implies that it is possible to reduce liquefaction induced structural settlement using basement storeys. This is currently being investigated using dynamic centrifuge modelling.

Archimedes' principle can be used to design a basement structure which will provide an uplift force equal to the weight of the structure when the surrounding soil liquefies, resulting in neutral buoyancy in the event of soil liquefaction.

The results from the first of a series of dynamic centrifuge model tests show that the presence of a basement, which was designed to provide neutral buoyancy, prevents the structure settling more than the far-field. However, the structure uplifted, which is also undesirable.

Further centrifuge model tests will be conducted to optimise the basement depth to achieve zero relative settlement compared to the far-field. The stability of the structure will also be considered. Particle image velocimetry (PIV) will be utilised in a number of future tests to further investigate the dominant mechanisms.

7 ACKNOWLEDGEMENTS

The first author would like to thank the Engineering and Physical Sciences Research Council (EPSRC) for their financial support. The first author would also like to thank the Earthquake Engineering Field Investigation Team (EEFIT) for enabling and financially supporting her participation in their reconnaissance mission to Ecuador, and the members of the mission for making it an invaluable learning experience.

8 REFERENCES

Allmond, J. & Kutter, B., 2014. Fluid Effects on Rocking Foundations in Difficult Soil. In *10th U.S. National Conference on Earthquake Engineering*. Anchorage, Alaska.

Bertalot, D., Brennan, A.J. & Villalobos, F.A., 2013. Influence of bearing pressure on liquefaction-induced settlement of shallow foundations. *Géotechnique*, 63(5), pp.391–399.

Brennan, A.J.A.J. et al., 2005. Evaluation of Shear Modulus and Damping in Dynamic Centrifuge Tests. *Journal of Geotechnical and Geoenvironmental Engineering*, 131(12), pp.1488–1497.

Brennan, A.J., Madabhushi, S.P.G. & Houghton, N.E., 2006. Comparing laminar and equivalent shear beam (ESB) containers for dynamic centrifuge modelling. In *6th International Conference on Physical Modelling in Geotechnics*. Hong Kong, pp. 171–176.

Chian, S.C. & Madabhushi, S.P.G., 2012. Excess pore pressures around underground structures following earthquake induced liquefaction. *International Journal of Geotechnical Earthquake Engineering*, 3(2), pp.25–41.

Dashti, S. et al., 2010. Mechanisms of Seismically Induced Settlement of Buildings with Shallow Foundations on Liquefiable Soil. *Journal of Geotechnical and Geoenvironmental Engineering*, 136(1), pp.151–164.

Franco, G. et al., 2017. The April 16 2016 MW 7.8 Muisne Earthquake in Ecuador - Preliminary Oberservation from the EEFIT Reconnaissance Mission of May 24 - June 7. In *16th World Conference on Earthquake Engineering*. Santiago, Chile.

Koseki, J., Matsuo, O. & Koga, Y., 1997. Uplift behaviour of underground structures caused by liquefaction of surrounding soil during earthquake. *Soils and Foundations*, 37(1), pp.97–108.

Madabhushi, G.S.P. & Haigh, S.K., 2012. How Well Do We Understand Earthquake Induced Liquefaction? *Indian Geotechnical Journal*, 42(3), pp.150–160.

Madabhushi, S.P.G., Houghton, N.E. & Haigh, S.K., 2006. A new automatic sand pourer for model preparation at University of Cambridge. In *Physical Modelling in Geotechnics*. Hong Kong, pp. 217–222.

Madabhushi, S.P.G., Schofield, A.N. & Lesley, S., 1998. A new stored angular momentum (SAM) based earthquake actuator. In *Proceedings of the International Conference Centrifuge 98*. pp. 111–116.

Mitrani, H. & Madabhushi, S.P.G., 2010. Cementation liquefaction remediation for existing buildings. *Proceedings of the ICE - Ground Improvement*, 163(2), pp.81–94.

O'Rourke, T.D. et al., 2014. Earthquake response of underground pipeline networks in Christchurch, NZ. *Earthquake Spectra*, 30(1), pp.183–204.

Schofield, A.N., 1980. Cambridge Geotechnical Centrifuge Operations. *Géotechnique*, 30(3), pp.227–268.

Schofield, A.N., 1981. Dynamic and Earthquake Geotechnical Centrifuge Modelling. In *Proceedings of the First International Conference on Recent Advances in Geotechnical Earthquake Engineering and Soil Dynamics*. St. Louis, Missouri, US, pp. 1081–1100.

Tomlinson, M.J., 2001. *Foundation design and construction* 7th ed., Prentice Hall.

Zeybek, A. & Madabhushi, S.P.G., 2016. Centrifuge testing to evaluate the liquefaction response of air-injected partially saturated soils beneath shallow foundations. *Bulletin of Earthquake Engineering*, 15(1), pp.339–356.